Turkish J. Eng. Env. Sci.
30 (2006) , 323 – 330.

Boundary Element Analysis of Interference Fits

Bahattin KANBER
University of Gaziantep, Mechanical Engineering Department, Gaziantep-TURKEY
e-mail: Kanber@gantep.edu.tr

Received 27.03.2006

Abstract

This paper presents the boundary element analysis of interference fit problems using axisymmetric boundary elements. A subregional technique is used to calculate the interference pressure and to find the von Mises stresses on the hub bore, without using iteration and incremental methods. The shaft and hub are modelled with equal lengths, unequal lengths, a shoulder on the shaft, and a grooved hub. Axisymmetric models of the shaft and hub are used to determine variable interference pressure along the interface line in the axial direction. The hub material is considered as steel and grey cast iron, and the shaft material is taken to be steel. All models used in the analysis are also solved using the finite element method with the ANSYS program. The results are compared with each other.

Key words: Interference fits, Subregional technique, Boundary element methods.

Introduction

Gears, pulleys, wheels, and similar elements are often assembled on a shaft by means of a press fit or shrink fit. A press fit, or force fit, is obtained by forcing a shaft into a smaller hole. A shrink fit is produced by heating the member having the hole and allowing it to cool to the shaft in ambient temperature. The radial interference is the difference between the change in radii of the hub and shaft. It can be calculated by multiplying the dimensionless interference (e) and the diameter of the shaft (d). Regardless of the fitting method, an interference fit creates an interference pressure, p, between the 2 parts. The stresses resulting from the interference pressure, in either part, at any radial position, can be calculated using Lame's equation (see Avallone and Baumeister, 1964).

The study by Zhang et al. (2000) shows that Lame's equation has some limitations. It was developed based on the study of thick-wall cylinder interference fits and 2-dimensional stress analysis for elastic loading; therefore, it is not suited for the design of press or shrink-fitted members in which the interference pressure is not constant along the interface line in the axial direction. The interference pressure can be different because of some geometric changes, such as unequal tube lengths, a shaft with a shoulder, and a grooved hub.

Some experimental methods can be used to measure the interference pressure of these types of interference fit problems, as shown in the work by Lewis et al. (2005); however, experimental methods are expensive, time consuming, and have some difficulties measuring the interference pressure. Instead of using experimental techniques, some numerical methods can be used. The finite element (FE) and boundary element (BE) methods are widely used in the analysis of engineering problems, and each one has some advantages and disadvantages. In general, the advantages of the FE method can be summarized as follows: familiar mathematics is used in the derivation of FEs, thin shell analysis can be more accurately carried out using the FE method, and the FE solution matrix is symmetric and generally not fully populated. The advantages of the BE method can be also given as follows: less data preparation time is required, which is due to surface modelling, stresses are accurate because no further approximation is imposed on the solution at interior points, less com-

puter time and storage are required in BE solutions, the BE method is more suitable for contact problems (see Becker, 1992), the contact stresses are more accurate in the BE method because there is a lesser degree of approximation imposed on the solution and the surface tractions, which are fundamental in determining the contact pressures, and are calculated to the same degree of accuracy as the displacements, enabling accurate coupling of contact variables. The interference problems are a special form of contact problem in which the contact surfaces are initially interfered.

In this study, interference fit problems are analysed using a subregional technique in the BE method, without using any iteration or incremental method. The hub materials are considered steel and grey cast iron. The shaft material is taken to be steel. The interference pressure is variable in the shaft and hub models along the axial direction. The BE solutions are compared with the FE solutions in the ANSYS program. The interference pressure distributions along the interface line in the axial direction and the von Mises stresses in the hub bore are illustrated against various interferences and d/D ratios.

Standards and Analytical Equations

The amount of interference needed to create a tight fit varies with the diameter of the shaft and the application. There are 2 standards for fits and tolerances, one based on inch units (ANSI B4.1-1967, R87) and the other on metric units (ANSI B4.2-1978, R94) (see Avallone and Baumeister, 1996). These standards contain detailed recommendations on fits and tolerances and serve as valuable guides for determining the required fit for a given application. In these standards, the interference fits are characterised by approximate constant bore pressures and are mainly classified as follows: locational interference fits (H7/p6-P7/h6), medium drive fits (H7/s6-S7/h6), and force fits (H7/u6-U7/h6).

The equation for interference pressure on a hub-shaft press-fitted assembly (Figure 1) can be obtained from thick-walled cylinder equations (see Shigley, 1986) as follows:

$$P = \frac{2e}{\frac{1-\nu_s}{E_s} + \frac{(2e-1)((1+\nu_h)D^2 - d^2(1-2e)^2(\nu_h-1))}{E_h((1-2e)^2\ d^2 - D^2)}} \qquad (1)$$

where e is the interference per meter of shaft diameter, D is the hub diameter, d is the shaft diameter, E_s and E_h are the elasticity moduluses of the shaft and hub, and ν_s and ν_h are the Poisson's ratios of the shaft and hub.

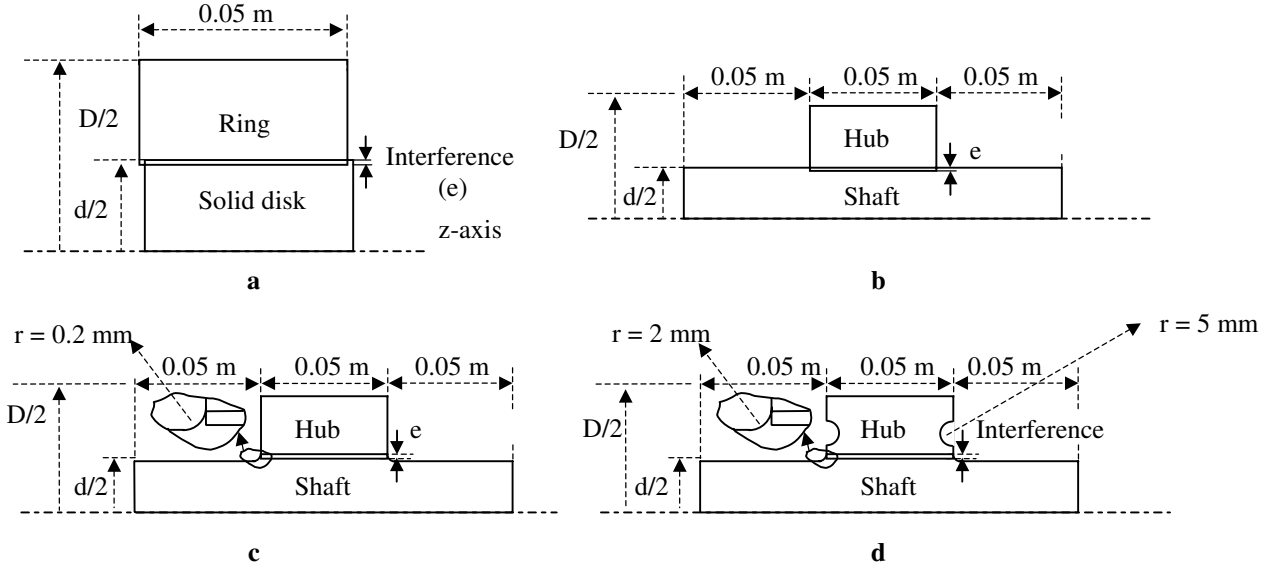

Figure 1. Axisymmetric models of **a**) Solid disk (shaft) and outer ring (hub), **b**) Shaft and hub, **c**) Shaft with shoulder and hub, **d**) Shaft with shoulder and grooved hub.

Then, the radial, tangential, and von Mises stresses on the hub can be written as follows:

$$\sigma_r = \frac{d^2 P}{D^2 - d^2}(1 - \frac{D^2}{r^2}) \tag{2}$$

$$\sigma_t = \frac{d^2 P}{D^2 - d^2}(1 + \frac{D^2}{r^2}) \tag{3}$$

$$\sigma_{VM} = \frac{1}{\sqrt{2}}\sqrt{(\sigma_r - \sigma_t)^2 + \sigma_r^2 + \sigma_t^2} \tag{4}$$

For the shaft (solid disk), they are equal to minus interference pressure.

Boundary Element Analysis

The general boundary integral equations for axisymmetric problems can be written as follows (see Becker, 1992):

$$\begin{bmatrix} u_r(p) \\ u_z(p) \end{bmatrix} + 2\pi \int_\Gamma \begin{bmatrix} T_{rr}(p,Q) & T_{rz}(p,Q) \\ T_{zr}(p,Q) & T_{zz}(p,Q) \end{bmatrix} \begin{bmatrix} u_r(Q) \\ u_z(Q) \end{bmatrix} r_Q \, d\Gamma(Q) = 2\pi \int_\Gamma \begin{bmatrix} U_{rr}(p,Q) & U_{rz}(p,Q) \\ U_{zr}(p,Q) & U_{zz}(p,Q) \end{bmatrix} \begin{bmatrix} t_r(Q) \\ t_z(Q) \end{bmatrix} r_Q \, d\Gamma(Q) \tag{5}$$

where p is an interior load point, Q is the field point, Γ is the boundary of the domain, r_Q is the radial coordinate of the field point, u_r and u_z are the radial and axial displacements, and t_r and t_z are radial and axial tractions. The boundary of the solution domain, Γ, must be divided into a number of connected elements. The following quadratic shape functions can be used for the geometry of the element (Figure 2) and the solution variables:

$$\begin{aligned} N_1(\xi) &= \tfrac{-\xi}{2}(1 - \xi) \\ N_2(\xi) &= (1 + \xi)(1 - \xi) \\ N_3(\xi) &= \tfrac{\xi}{2}(1 + \xi) \end{aligned} \tag{6}$$

where ξ are the local coordinates. The displacement kernels (U_{ij}), traction kernels (T_{ij}), and other programming details of the procedure can be found in the book by Becker (1992).

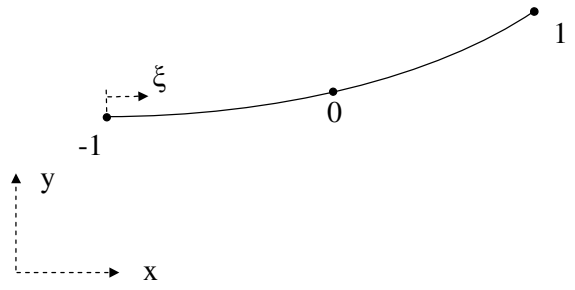

Figure 2. An isoparametric quadratic boundary element.

Equation (5) can be written in a compact form as follows:

$$[A] \;\; [u] = [B] \;\; [t] \tag{7}$$

The press-fit problems generally include a shaft and a hub, and Eq. (7) can be written for a shaft and hub as follows:

$$[A]^s \;\; [u]^s = [B]^s \;\; [t]^s \tag{8}$$

and

$$[A]^h \;\; [u]^h = [B]^h \;\; [t]^h \tag{9}$$

where the superscripts s and h refer to the shaft and hub, $[u]^s$ and $[u]^h$ are the displacement, and $[t]^s$ and $[t]^h$ are the traction vectors in the domain of the shaft and hub.

The continuity and the equilibrium requirements can be satisfied without friction at the interface of the shaft and hub as follows:

$$u_{ri}^s = u_{ri}^h + e * d \tag{10}$$

$$t_{ri}^s = -t_{ri}^h = P \tag{11}$$

where u_{ri}^s and u_{ri}^h are the radial displacements at the interface line of the shaft and hub, t_{ri}^s and t_{ri}^h are the radial tractions, and P is the interference pressure at the interface line of the shaft and hub. Equations (8) and (9) can be rewritten by using the interface and remaining boundary sub-matrices as follows:

$$\left[[A]^s [A]_{ri}^s\right] \begin{bmatrix} [u]^s \\ [u]_{ri}^s \end{bmatrix} = \left[[B]^s [B]_{ri}^s\right] \begin{bmatrix} [t]^s \\ [P] \end{bmatrix} \tag{12}$$

$$\left[[A]^h [A]_{ri}^h\right] \begin{bmatrix} [u]^h \\ [u]_{ri}^h \end{bmatrix} = \left[[B]^h [B]_{ri}^h\right] \begin{bmatrix} [t]^h \\ -[P] \end{bmatrix} \tag{13}$$

where $[A]_{ri}^s$, $[B]_{ri}^s$, $[A]_{ri}^h$, and $[B]_{ri}^h$ are the submatrices at the interface line. The interference pressure can be found by a load incremental approach; however, if Eqs. (12) and (13) are combined, the solution can be directly carried out using the ordinary Gauss elimination approach. To combine them, the continuity and equilibrium equations can be used

(Eqs. (10) and (11)). If the prescribed tractions are considered zero, the whole matrix becomes:

$$\begin{bmatrix} [A]^s & [0] & -[B]^s_{ri} \\ [0] & [A]^h & [B]^h_{ri} \\ [uc]^s_{ri} & [uc]^h_{ri} & [0] \end{bmatrix} \begin{bmatrix} [u]^s \\ [u]^h \\ [P] \end{bmatrix} = \begin{bmatrix} [0] \\ [0] \\ [e*d] \end{bmatrix} \tag{14}$$

where $[uc]^s_{ri}$ and $[uc]^h_{ri}$ are the sub-matrices, which include zero elements when the position of an element does not correspond to a relevant interface normal displacement. When an element corresponds to an interface normal displacement it becomes 1. Therefore, Eq. (14) becomes a rectangular matrix and all unknowns are collected in the left-hand side. The ordinary Gauss elimination approach can be used to find the interface tractions. The matrix in Eq. (14) is not fully populated and includes zero elements. This causes unnecessary memory requirements. Some further arrangements may be done to prevent this.

After finding the unknown interface tractions, the interface displacements can be found by solving Eqs. (12) and (13). Then, the strain components at the nodes at the hub interface line can be obtained using the following equations:

$$\varepsilon^h_{ri}(\xi) = \frac{1}{J(\xi)} \left\{ \left[\sum_{c=1}^{3} \frac{\partial N_c(\xi)}{\partial \xi} (u^h_{ri}) \right] \right\},$$

$$\varepsilon^h_{zi}(\xi) = \frac{1}{J(\xi)} \left\{ \left[\sum_{c=1}^{3} \frac{\partial N_c(\xi)}{\partial \xi} (u^h_{zi}) \right] \right\} \tag{15}$$

where u^h_{zi} represents the tangential displacement components at the interface line, which are already included in the sub-matrices u^h in Eq. (13). N_c represents the shape functions and $J(\xi)$ is the Jacobian matrix, which gives the relationships between local (ξ) and global coordinate systems (r, z).

Then, the stress components at the hub interface line can be directly calculated using the following equations:

$$\begin{aligned} \sigma^h_{zi} &= \left(\tfrac{E}{1-\nu^2}\right)\left(\varepsilon^h_{zi} + \nu\varepsilon^h_{\theta i}\right) + \left(\tfrac{\nu}{1-\nu}\right) t^h_{zi} \\ \sigma^h_{ri} &= t^h_{ri} \\ \sigma^h_{zri} &= t^h_{zi} \\ \sigma^h_{\theta i} &= E\varepsilon^h_{\theta i} + \nu(\sigma^h_{zi} + \sigma^h_{ri}) \end{aligned} \tag{16}$$

where t^h_{zi} is the tangential traction components at the hub interface line, which are already included in the sub-matrices t^h in Eq. (13). $\sigma^h_{\theta i}$ and $\varepsilon^h_{\theta i}$ are hoop stresses and strains, and $\varepsilon^h_{\theta i} = \frac{u^h_{ri}}{r^h_i}$.

An existing BE program, BEACON (see Becker, 1992), has been improved using Eqs. (8), (9), and (16) for solving interference fit problems. This program can solve 2-dimensional and axisymmetric elastostatic problems using 3-noded isoparametric quadratic BEs (Figure 2). It has been improved using the FORTRAN 95 programming language. In this program, the maximum number of nodes and elements can be automatically determined by a module called Coblock. Semi-dynamic arrays were used to handle matrices and vectors. A modular programming technique was used in the program, using explicit external subroutines.

Finite Element Analysis

Axisymmetric FE models were created using ANSYS finite element analysis software, as in the BE method. Uniform and regular meshes were used. The shaft and hub were modelled using PLANE82 8-node rectangular elements with an axisymmetric option. The interface region of the hub and shaft was modelled using surface-to-surface contact elements, without friction (TARGE169 and CONTA172). Regardless of the fitting method (shrink or press fit), the amount of interference was given as an initial penetration. The radius of the shaft was given as larger than the hub bore radius in an amount of interference, as shown in Figure 1. The symmetry line was chosen as the y-axis. After generation of contact elements, the solution was directly started as small displacement static. Due to geometric non-linearity, the full Newton-Raphson iteration method was used in the solution. The solver type was the sparse matrix direct solver.

Solutions and Discussions

All models were solved with a PC. The hardware configuration consisted of an Intel Pentium IV 2.4 GHz CPU and 1 GB of RAM. Although the aim of this study is calculating the interference fit pressures accurately, CPU time comparisons can also be done as shown in Table 1. CPU time completely depends on the solver type. Therefore, ANSYS was forced to use the Frontal direct solver. In the BE program, however, an ordinary Gauss elimination solver was used with a subregional approach. Although the

Table 1. CPU time comparison.

	ANSYS (With Frontal Direct Solver)	BEM (With Ordinary Gauss Elimination Solver)
Shaft and hub with equal tube lengths (Figure 1a)	351 s (17,746 nodes)	4 s (156 nodes)
Shaft and hub with unequal tube lengths (Figure 1b)	353 s (23,986 nodes)	36 s (1089 nodes)
Shaft with shoulder and hub (Figure 1c)	173 s (30,362 nodes)	8 s (359 nodes)
Shaft with shoulder and grooved hub (Figure 1d)	172 s (22,074 nodes)	12 s (509 nodes)

CPU times of BE solutions is less than ANSYS solutions, it is completely the result of the number of nodes in the models. If ANSYS is permitted to use its default solver, CPU times can be decreased further. In Table 1, CPU times of the third (Figure 1c) and fourth FE models (Figure 1d) are nearly the same; however, the number of nodes are very different. The reason for this difference is the number of nodes in the contact area.

Four different configurations were used for shaft and hub assembly. In the first one, a solid disk and an outer ring were modelled with equal tube lengths (Figure 1a). In the FE model, 17,746 nodes were used. In the BE model, only 156 nodes were used. Quadratic finite and boundary elements were used in all models. Analytical solutions were carried out using Eqs. (1)-(4). The interference pressure is directly equal to the radial stress at the interface line. The variations of interference pressure and von Mises stresses along axial direction were represented in all plots. The interference pressures and von Mises stresses are in good agreement in all methods, as shown in Figures 3 and 4. In spite of plenty of nodes in the FE model, the stresses show some deviations at the corner nodes at the interface line. The corners of the hub were not rounded in the model, which causes these stress deviations at this point. It is a usual problem in FE solutions. If the corners of the hub are rounded using some small radius fillets, these errors can be removed; however, BE models give nearly the same results with analytical solutions. In order to show the correctness of the BE solutions, FE models were kept in their original shapes.

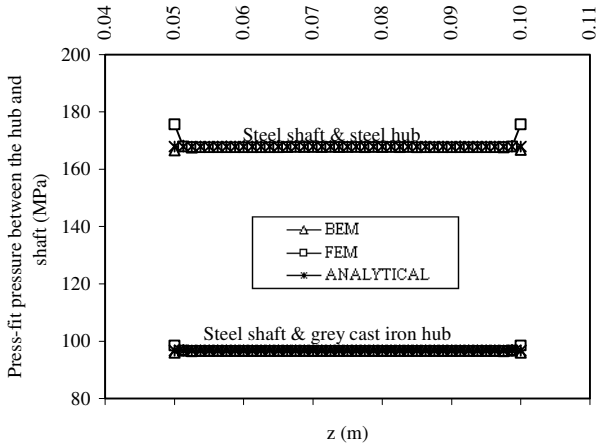

Figure 3. Press fit pressure distributions along the hub bore, while d/D = 0.4 and e = 0.001 (shaft and hub with equal tube lengths-Figure 1a).

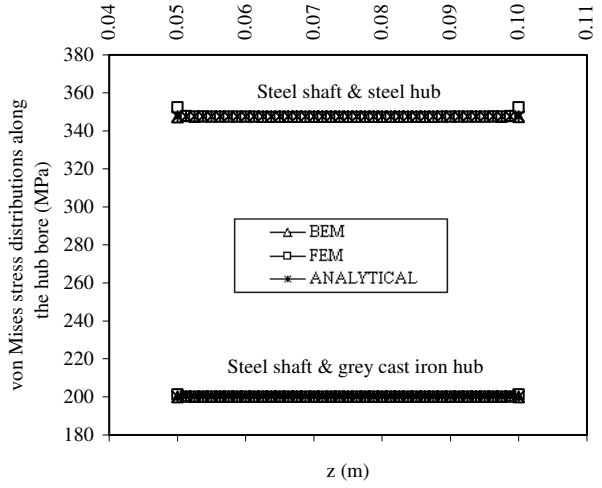

Figure 4. Von Mises stress distributions along the hub bore, while d/D = 0.4 and e = 0.001 (shaft and hub with equal tube lengths-Figure 1a).

In the second model, a shaft and hub assembly was modelled with unequal tube lengths, as shown in Figure 1b. In the FE and BE models, 23,986 nodes and 1089 nodes were used, respectively. The FE and BE results are in good agreement, as shown in Figures 5 and 6. The interference pressures at the interface line and the von Mises stresses along the hub bore are nearly equal to the pressures and stresses obtained in the first model, except for the corner nodes. At the corner nodes there is a stress concentration and the failure begins from these points during loading.

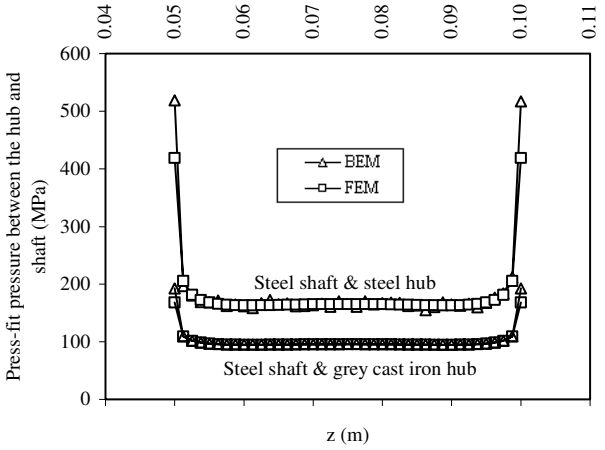

Figure 5. Press fit pressure distributions along the hub bore, while d/D = 0.4 and e = 0.001 (shaft and hub with unequal tube lengths-Figure 1b).

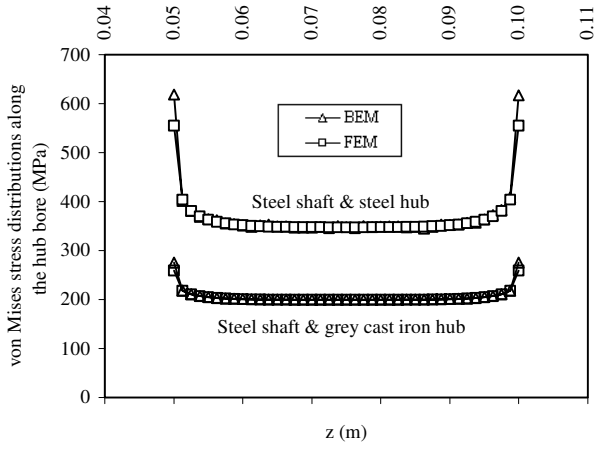

Figure 6. Von Mises stress distributions along the hub bore, while d/D = 0.4 and e = 0.001 (shaft and hub with unequal tube lengths-Figure 1b).

The corner stresses in the second model are the main concern of many researchers and are solved by considering a shoulder in the shaft (see Pilkey, 1997). This is the third model as shown in Figure 1c. A shaft is modelled with a shoulder with a 0.2 mm radius. The remaining geometry is the same as that in the previous model. In the FE and BE models, 30,362 nodes and 359 nodes were used, respectively. The BE solutions show that the interference pressure was reduced 50% and von Mises stress was reduced 30% for the steel shaft and hub, as shown in Figures 7 and 8. The interference pressure was reduced 40% and von Mises stress was reduced 25% for the grey cast iron hub and steel shaft, as shown in the same figures.

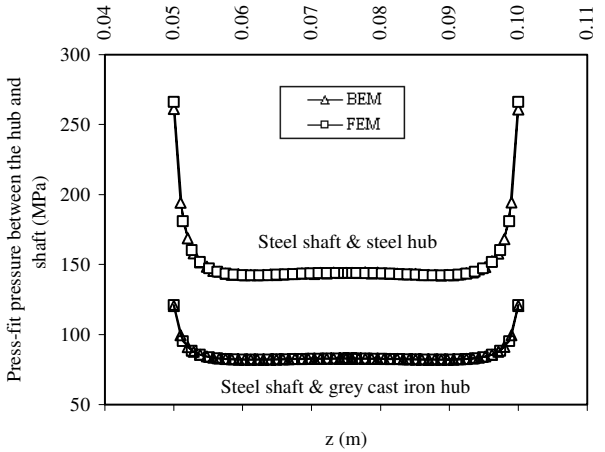

Figure 7. Press fit pressure distributions along the hub bore, while d/D = 0.4 and e = 0.001 (shaft with shoulder and hub-Figure 1c).

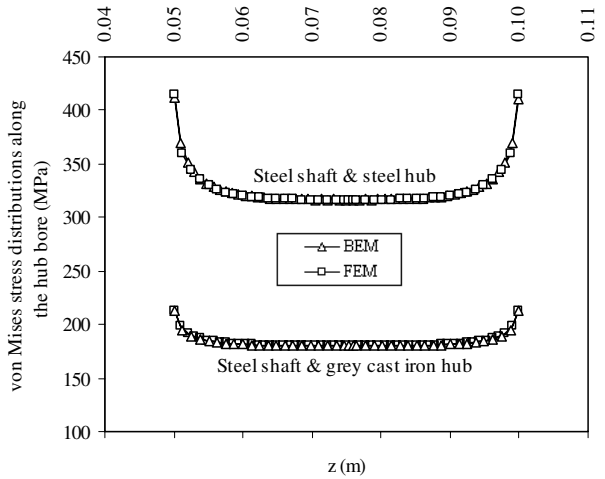

Figure 8. Von Mises stress distributions along the hub bore, while d/D = 0.4 and e = 0.001 (shaft with shoulder and hub-Figure 1c).

The last model includes a grooved hub and a shaft with a shoulder. The groove radius is 5 mm and shoulder radius is 0.2 mm, as shown in Figure 1d. In the FE and BE models, 22,074 nodes and 509 nodes were used, respectively. Both FE and BE solutions show that the stress concentrations at the hub corners were completely removed and the maximum von Mises stress was reduced by 15% of the previous model (Figures 9 and 10). Similar results were obtained for the grey cast iron hub and steel shaft. BE solutions give minus pressures at the hub corners for both steel and grey cast iron, as shown in Figure 9. In order to investigate the correctness of these results, a fine BE model was solved with 1032 nodes. The results do not include any negative pressures, as shown in Figure 9. Consequently, the results of the coarse model include some errors at the corner nodes. This may be caused by the size of BEs around the corners. In the BE element program, which was used in this study, the A and B matrices were constructed based on element sub-matrices, as shown in Eq. (14) and so the size of BE directly affects the nodal results. Figure 3 shows that both FE and BE results include some errors at the corner nodes and that they are in good agreement at the remaining nodes; however, the BE results are closer to the analytical results than the FE results.

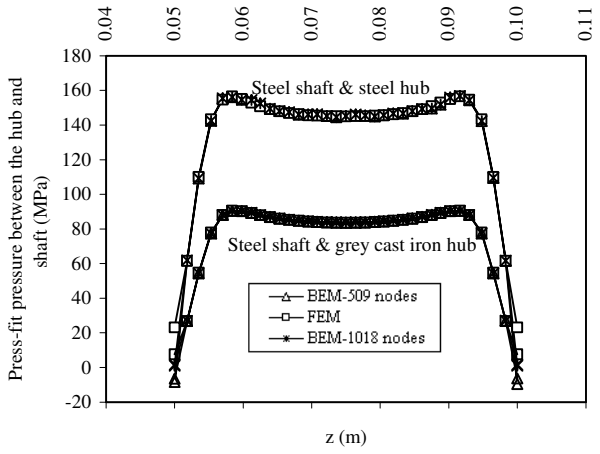

Figure 9. Press fit pressure distributions along the hub bore while d/D = 0.4 and e = 0.001 (shaft with shoulder and grooved hub-Figure 1d).

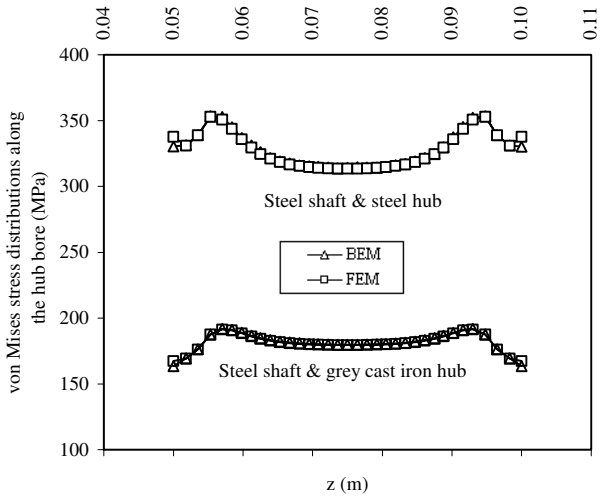

Figure 10. Von Mises stress distributions along the hub bore, while d/D = 0.4 and e = 0.001 (shaft with shoulder and grooved hub-Figure 1d).

Conclusions

The interference fit problems are analysed using axisymmetric boundary elements and a subregional technique. It was shown that the BE method is a more suitable method to analyse press fit problems. Its results are more accurate than the FE method, in spite of less mesh data.

The hub material selected was steel and grey cast iron. The grey cast iron hub reduces the interface pressures and von Mises stresses; yet, it must be carefully examined by considering the external loads and design considerations.

The interference pressure and von Misses stress concentrations at the corners of the hub can be reduced using shoulders on the shaft and their distribution may be changed by grooved hubs. Various designs can be developed by changing the radius of the shoulders on the shaft and the grooves on the hub.

Nomenclature

e	interference per metre of shaft diameter
D	hub diameter
d	shaft diameter
E_s, E_h	elasticity moduluses of the shaft and hub
ν_s, ν_h	Poisson's ratios of the shaft and hub

$\sigma_r, \sigma_t, \sigma_{VM}$	radial, tangential, and von Mises stresses
p, Q	interior load point and field point
Γ	boundary of the domain
r_Q	radial coordinate of the field point
u_r, u_z	radial and axial displacements
t_r, t_z	radial and axial tractions
U_{ij}, T_{ij}	displacement and traction kernels
$[u]^s, [u]^h$	displacement vectors in the domain of the shaft and hub
$[t]^s, [t]^h$	traction vectors in the domain of the shaft and hub
u^s_{ri}, u^h_{ri}	radial displacements at the interface line of the shaft and hub
t^s_{ri}, t^h_{ri}	radial tractions
P	interference pressure at the interface line of the shaft and hub
$[A]^s_{ri}, [A]^h_{ri}$	sub-matrices, including displacement kernel terms
$[B]^s_{ri}, [B]^h_{ri}$	sub-matrices, including traction kernel terms
$[uc]^s_{ri}, [uc]^h_{ri}$	sub-matrices, including zero and one
$\varepsilon^h_{ri}, \varepsilon^h_{zi}$	strain components at the nodes at the hub interface line
u^h_{zi}	tangential displacement components at the interface line
$J(\xi)$	Jacobian matrix
ξ	local coordinates
$N_c(\xi)$	shape functions
$\sigma^h_{zi}, \sigma^h_{ri}, \sigma^h_{zri}$	tangential, radial, and shear stress components at the hub interface
$\sigma^h_{\theta i}, \varepsilon^h_{\theta i}$	hoop stresses and strains

References

Avallone, E.A. and Baumeister III, T., Mechanical Design and System Handbook, McGraw-Hill, New York, 1964.

Avallone, E.A. and Baumeister III, T., Marks' Standard Handbook for Mechanical Engineers, McGraw-Hill, New York, 1996.

Becker, A.A., The Boundary Element Method in Engineering, McGraw-Hill, Cambridge, 1992.

Lewis, R., Marshall, M.B. and Dwyer-Joyce, R.S., "Measurement of Interface Pressure in Interference Fits", Proc. IMechE PartC: J. Mechanical Engineering Science, 219, 127-139, 2005.

Pilkey, W.D., Peterson's Stress Concentration Factors, John Wiley & Sons, New York, 1997.

Shigley, J.E., Mechanical Engineering Design, McGraw-Hill, New York, 1986.

Zhang Y., McClain B. and Fang X.D., "Design of Interference Fits via Finite Element Method", International Journal of Mechanical Sciences, 42, 1835-1850, 2000.